Green Chemistry

PAPER

View Article Online
View Journal | View Issue

Cite this: *Green Chem.*, 2024, **26**, 4528

Preparation of homogeneous lignin nanoparticles by efficient extraction of lignin and modification of its molecular structure using a functional deep eutectic solvent containing γ-valerolactone†

Mingzhu Yao,[a] Baojie Liu,[a] Lina Qin,[a] Zicheng Du,[a] Zenglin Wang,[a] Chengrong Qin,[a] Chen Liang,[a] Caoxing Huang[b] and Shuangquan Yao *[a]

Deep eutectic solvents (DESs) are widely used as recyclable green solvents for the separation of lignin from lignocellulosic biomass. However, the poor permeability of DES solution limits the green advancement of separation systems. In addition, lignin fragment molecules are susceptible to repolymerization reactions during separation, resulting in reduced lignin reactivity. In this study, a DES consisting of choline chloride (ChCl) as a hydrogen acceptor, 5-sulfosalicylic acid (5Saa) as a hydrogen donor, and a certain amount of γ-valerolactone (GVL) as an additive was designed. The system not only efficiently fractionated lignin from poplar (71.35%), but also selectively retained almost complete cellulose (retention 92.87%) under the optimal fractionation (ChCl/5Saa/GVL molar ratio 1/4/15, temperature 120 °C, time 3.0 h). Pre-crushing processing of raw materials was avoided as the new DES solution has stronger permeability compared to the previous DES solution. Selective deconstruction of lignocellulose was achieved due to a strong hydrogen network structure. The lignin fragments were effectively dissolved. The results showed that the stability of the carbo-positive active intermediates was enhanced by ChCl–5Saa/GVL. Lignin with a low molecular weight (2305 g mol^{-1}), high purity (98.77%) and high total phenolic hydroxyl content (6.92 mmol g^{-1}) was obtained. Homogeneous lignin nanoparticles (LNPs) were prepared with an average particle size of 23 nm. LNPs had high dispersion stability and excellent UV shielding properties. The green advancement of the new DES has been significantly improved and the efficient fractionation of high-value lignin was realized.

Received 12th December 2023,
Accepted 28th February 2024

DOI: 10.1039/d3gc04897g

rsc.li/greenchem

Introduction

Separation of lignocellulosic biomass using green separation technologies offers more possibilities for biomass utilization.[1,2] In particular, due to its special structural and functional properties, lignin is one of the most promising renewable resources.[3,4] Its monomers have an aromatic compound structure containing phenolic hydroxyl and carboxyl reactive groups.[5] The lignin-derived aromatic hydrocarbons produced after hydrogenolysis can be used as fuel instead of gasoline, and monophenols can replace phenol in the production of adhesives and other chemical products.[6,7] In addition, polyphenolic lignin can be used as a sensitizer for thin film electrodes in solar chemical cells.[8,9] Therefore, it is important to efficiently and selectively isolate lignin with high added value.[10,11] Using DESs is considered one of the effective methods for green separation of lignin because of their good thermal stability, recyclability and biodegradability.[12–14] A strong hydrogen bonding network structure is formed in DESs through the interaction between a hydrogen donor (HBD) and a hydrogen acceptor (HBA).[15] Lignin depolymerization and segregation are achieved by cleaving unstable aryl ether bonds.[16,17] However, the formation of carbon–carbon bonds makes lignin more structurally complex and less reactive. It limits the value of lignin for applications in fuels and chemical and material manufacturing.[18] This implies that the heterogeneity of the molecular structure of lignin is a challenge for efficient fractionation and high-quality conversion of lignin by using DESs.

Currently, acidic DES systems have an excellent lignin separation ability. Generally, such a system is composed of choline chloride (ChCl) as the HBA and an organic acid as the

[a]*Guangxi Key Laboratory of Clean Pulp & Papermaking and Pollution Control, School of Light Industrial and Food Engineering, Guangxi University, Nanning, 530004, PR China. E-mail: yaoshuangquan@gxu.edu.cn*
[b]*Jiangsu Co-Innovation Center of Efficient Processing and Utilization of Forest Resources, Nanjing Forestry University, Nanjing, 210037, PR China*
† Electronic supplementary information (ESI) available. See DOI: https://doi.org/10.1039/d3gc04897g

HBD. Hong *et al.*[19] utilized choline chloride–lactic acid (ChCl–LA) and choline chloride–oxalic acid (ChCl–OA) systems for the separation of poplar. The separation efficiency of lignin was 44–75%. It was shown that the HBD was the key to break the ether bond connection between the phenylpropane units. This was attributed to the fact that the number of oxygen atoms of the HBD significantly affects the strength of the DES hydrogen bonding network and its hydrogen bonding interaction with lignin. This implies that modulation of the HBD is one of the effective means to enhance the separation efficiency of lignin. Tan *et al.*[20] comparatively analyzed the separation efficiency of DESs with different HBD compositions for lignin. It was found that HBDs containing carboxyl and hydroxyl structures were more effective for lignin separation. However, HBDs with a single functional structure were employed in previous studies. In particular, commonly used carboxylic acid- and polyol-based DESs contain only the COOH or OH group. This is responsible for the weak permeability nature of conventional DESs to efficiently break down cell walls. In fact, the pulverization pretreatment of the feedstock (20–80 mesh wood flour) was used as an adjunct to the DES separation technology. Obviously, the green and efficient separation value of DES treatment was reduced. Therefore, the choice of the HBD has a significant impact on the lignin separation efficiency. Fortunately, 5-sulfosalicylic acid (5Saa) is a green, mild organic acid rich in carboxyl and hydroxyl groups. It has a high pK_a value with an excellent osmotic effect.[21] New strong hydrogen bonds will be formed along with the reaction of the phenyl-containing DES with lignin.[22] The complex network of hydrogen bonds in lignocellulosic biomass will be efficiently disrupted utilizing strong hydrogen bonding. This means that the separation efficiency of lignin will be enhanced. In addition, crushing pretreatment of the raw material will be avoided due to the new DES permeability enhancement. The green advancement of DESs has been effectively enhanced. This not only simplifies the separation process, but also reduces the energy consumption for separation. Furthermore, the regulation of the lignin molecular structure has been neglected during DES separation.[15] Lignin side-chain carbo-positive active intermediates could attack the electron-rich aromatic ring of lignin during the separation process.[5] The stabilized carbon–carbon bonds between lignin molecules were formed, limiting the processability and availability of lignin.[23] Therefore, the regulation of the lignin molecular structure is an important measure for its efficient separation and high value utilization of lignin in DES separation. Recently, the stabilizing effect of γ-valerolactone (GVL), a sugar-derived derivative and polar nonprotonic solvent, has been discovered on carbo-positive active intermediates.[24,25] Recombination of acid protons with their counterions will be facilitated. Furthermore, the lignin molecular structure could be efficiently regulated.[25] The decrease in the accessibility of the reactive cellulose surface is prevented. This suggests that the construction of a novel dual-effect DES system with both efficient lignin fractionation and lignin molecular structure modulation is a new strategy to achieve high-value utilization of lignin. This means that greener, more energy-efficient and more advanced DES processing will be realized.

In this study, a ternary DES system with a stable hydrogen-bonded macromolecular network structure was designed. It consisted of choline chloride ChCl, 5Saa, and GVL. The physicochemical properties and hydrogen bonding network structure of the functional novel DES system were investigated. Its selective separation of poplar lignin was analyzed. Molecular structural features and surface chemical properties of regenerated lignin were analyzed. In addition, the separation mechanism of lignin by the novel DES was investigated. Meanwhile, highly active lignin nanoparticles (LNPs) were prepared. It is promising for a wide range of applications in the field of functional materials. The results of the study will contribute to the efficient fractionation and high-quality conversion of lignin.

Results and discussion

Preparation and characterization of the DES

The nature of DESs greatly affects their separation efficiency, ability to delignify lignin, and structural changes in the separation of biomass fractions.[26] The good deconstruction of biomass fractions and solubilization of lignin are mainly attributed to the strong hydrogen-bonding network.[6,27] Therefore, the hydrogen bonding interactions in the different DES systems were analyzed. The ^{1}H NMR spectra of ChCl–Lac, ChCl–5Saa, and ChCl–5Saa/GVL at different concentrations (150 mg ml^{-1}, 100 mg ml^{-1}, and 50 mg ml^{-1}) are shown in Fig. 1a. The chemical shifts in the H-proton peaks of CH_2–CHN (1.78 ppm, 2.50 ppm, 3.00 ppm) in ChCl, H-proton peak of –CH_3 (1.30 ppm), and H-proton peak of the benzene ring (6.96 ppm, 7.80 ppm, 8.00 ppm) in GVL shifted significantly toward the high field as the solution concentration decreased. In fact, when the energy of hydrogen bonds changes, the proton signal shifts accordingly.[28] This suggests the formation of an intermolecular hydrogen-bonding network between the three substances in the ChCl–5Saa/GVL system. Similar phenomena were observed for ChCl–Lac and ChCl–5Saa. Moreover, the broad and tonal peak shape of the –OH stretching vibration peak at 3600–3000 cm^{-1} was observed in FTIR for the concentrated solution of the ChCl–5Saa/GVL solvent system (Fig. 1b). However, it exhibits a sharp and high peak shape in dilute solutions. This reveals the existence of a large number of intermolecular hydrogen-bonding network structures within all three DES systems.

The structure of the intermolecular hydrogen-bonded network affects the spatial arrangement of the molecules and charge delocalization.[29] The physicochemical properties (melting point, density, conductivity, and viscosity) of the DES are strongly influenced by hydrogen bonding. The melting point of ChCl–5Saa was 80 °C. But the melting point of ChCl–5Saa/GVL was 65 °C. This was attributed to the hydrogen bonding interaction formed between the new DES leading to charge delocalization, which brings about a significant

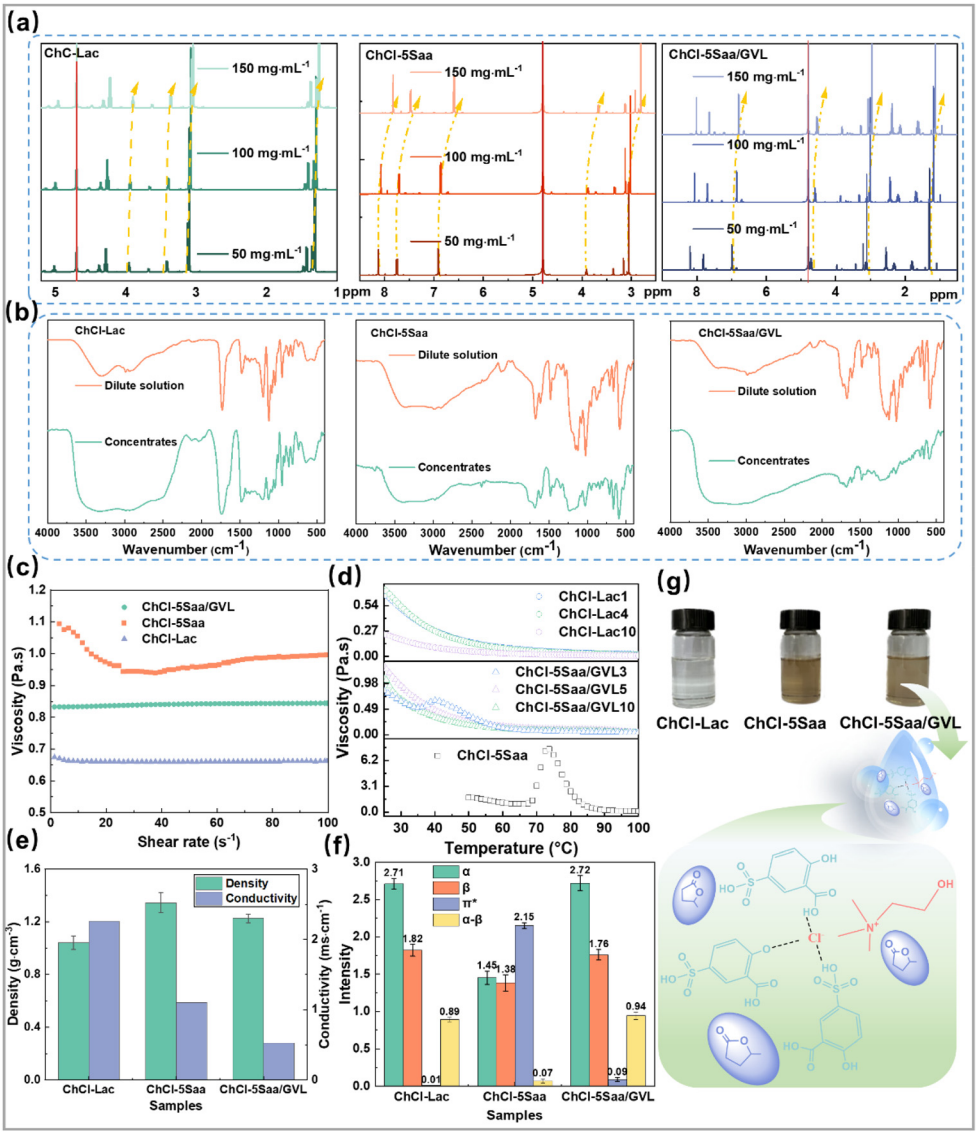

Fig. 1 Physicochemical properties and structural characteristics of different DES systems (ChCl–Lac, ChCl–5Saa, and ChCl–5Saa/GVL) ((a) ^{1}H NMR; (b) FTIR; (c) viscosity curves; (d) shear viscosity *versus* temperature curves, where ChCl–Lac with molar ratios of (1 : 1), (1 : 4), and (1 : 10) are denoted as ChCl–Lac1, ChCl–Lac4, and ChCl–Lac10, ChCl–5Saa with a molar ratio of (1 : 4) is denoted as ChCl–5Saa, and ChCl–5Saa/GVL with a molar ratio of (1 : 4 : 3), (1 : 4 : 5), and (1 : 4 : 10) is denoted as ChCl–5Saa/GVL3, ChCl–5Saa/GVL5, and ChCl–5Saa/GVL10, respectively; (e) density *versus* conductivity; (f) solvent discoloration parameters; (g) DES physical diagram and hydrogen bonding network structure of ChCl–5Saa/GVL).

reduction in the melting point.[30] As shown in Fig. 1e, the densities of ChCl–Lac, ChCl–5Saa, and ChCl–5Saa/GVL at 1.04 g cm^{-3}, 1.34 g cm^{-3}, and 1.23 g cm^{-3}, respectively, were similar. ChCl–5Saa's conductivity at 1.09 mS cm^{-1} was lower than that of ChCl–Lac. This is attributed to the presence of fewer free ions in the surface solution system. The hydrogen-bonding interaction forces of Ch^{+}–5Saa (anionic hydrogen bonding) and Cl^{-}–5Saa (cationic-ionic hydrogen bonding) were formed because of the interaction of the choline cation (Ch^{+}) in ChCl with the hydroxyl, carboxyl, and sulfonic groups of 5Saa. This led to a reduction in the number of free ions. In addition, the conductivity of ChCl–5Saa/GVL is as low as 0.53 mS cm^{-1}. This is half that of ChCl–5Saa. This was because the hydrogen bonding structure of the ChCl–5Saa system changed with the addition of GVL. As a nonprotonic solvent, GVL interfered with the stabilization of the acid site. Recombination of the acid proton with its counterion was prompted. This phenomenon is similar to the linear bead structure of water molecules entering the DES system to form "hydrated chlorides".[31] This implied the formation of a stable strong hydrogen bonding network structure in ChCl–5Saa/GVL (Fig. 1g).

The ChCl–5Saa system is extremely unstable at ambient temperatures. Viscosity experiments were conducted at 65 °C to ensure uniformity of experimental conditions. The results showed that the viscosity of the DES system was not very high. The viscosities of ChCl–Lac, ChCl–5Saa, and ChCl–5Saa/GVL

were 0.66 Pa s, 0.94 Pa s, and 0.84 Pa s, respectively (Fig. 1c). ChCl–Lac and ChCl–5Saa/GVL are Newtonian fluids. The shear rate had no effect on the solution's viscosity. However, ChCl–5Saa exhibits shear thinning, which indicates that it is a non-Newtonian fluid. The viscosity gradually tended to be constant when the shear rate exceeded 20 s^{-1}. Therefore, the effect of temperature on the viscosity of the DES system was studied at a shear rate of 30 s^{-1}. Fig. 1d shows that the viscosities of ChCl–Lac at different molar ratios (1 : 1, 1 : 4, and 1 : 10) gradually decreased with increasing temperature. In particular, the viscosity remained stable after the temperature exceeded 60 °C. This indicates that the ChCl–Lac system, in which Lac forms hydrogen bonds with Cl^-, is stable and shows homogeneous liquid properties.[32] However, ChCl–5Saa (1 : 4) and ChCl–5Saa/GVL (1 : 4 : 3) exhibited increased viscosity during shearing in the ranges of 70–85 °C and 35–45 °C, respectively. This is attributed to the instability of both solvent systems at ambient temperature. A freezing point was observed during the shear process, and some crystals precipitated. The crystals rapidly dissolved when the temperature exceeded the melting point of the mixture. This led to a decrease in the viscosity, which remained smooth. However, ChCl–5Saa/GVL (1 : 4 : 5) and ChCl–Lac (1 : 4 : 10) did not appear to have a freezing point, and both ratios had similar viscosity patterns. This suggests that stable ChCl–5Saa/GVL solvent systems could be prepared by modulating the molar ratio. In addition, the chemical properties of the different DES systems were quantified using the K–T parameters. Fig. 1f shows that the acidity (α) value, alkalinity (β) value, and polarizability (π^*) of ChCl–5Saa/GVL were similar to those of ChCl–Lac. These values are 2.72, 1.76, and 0.94, respectively. This indicates that the hydrogen bond donor capacity, hydrogen bond acceptor capacity, and polarization rate of the ChCl–5Saa/GVL system are similar to those of ChCl–Lac.[33] However, α, β, and π^* values of ChCl–5Saa were 1.45, 1.38, and 2.15, respectively. This is attributed to the fact that the hydrogen-bonding ability of the ChCl–5Saa system to release and accept H was enhanced by the addition of GVL. This contributes to the formation of a more uniform and stable hydrogen-bonding network structure in the ChCl–5Saa/GV system. Therefore, the ChCl–5Saa/GVL system exhibited strong stability and a hydrogen-bonding network structure. This implies that the catalytic reaction rate and solvent penetration properties were enhanced in lignocellulosic biomass separation.

Efficient fractionation of lignin from poplar wood

The ChCl–5Saa/GVL solvent system was used for the fractionation of poplar fractions. The reason for the high solubility of DESs is the high availability, permeability, and reactivity of hydrogen protons in such systems.[34] The molar ratios of hydrogen acceptor (HBA), hydrogen donor (HBD), and additives had a significant effect on the solubility of DESs.[22] First, the effect of the DES ratio of the new ternary DES (ChCl–5Saa/GVL) system on the lignin removal efficiency was studied at 100 °C for 2 h for 1 : 4 : 0, 1 : 4 : 3, 1 : 4 : 10, 1 : 4 : 15, 1 : 4 : 20, and 1 : 4 : 25. Fig. 2a shows that the lignin removal efficiency was 28.95% at a ratio of 1 : 4 : 0. It increased to 53.16% at a ratio of 1 : 4 : 15. The results clearly show that the lignin removal efficiency increased with an increase in GVL percentage. Importantly, the cellulose removal was negligible. This is attributed to the solubilizing effect of the ChCl–5Saa/GVL solvent system on lignin. ChCl acted as a hydrogen bonding acceptor. Since the hydroxyl, carboxyl and sulfonic acid groups in 5Saa provide H ions, it formed a strong hydrogen bonding network structure with ChCl.[35] Thus, the polarity and permeability of the solvent increased. This led to stronger interactions between the DES and the free/etherified hydroxyl groups in lignin.[20] Proton-catalyzed cleavage of ether bonds in lignocellulose and ester bonds in lignin–polysaccharide compounds was promoted. The cell wall of lignocellulosic biomass was easily cleaved. And when acidic protons were active in the catalyst, CVL accelerated the rate of the catalytic reaction.[36] Hydrogen bonding between the HBA (ChCl) and the HBD (5Saa) in the original binary system was enhanced with the increase in the GVL molar ratio. The change in the solvent properties of the new ternary solvent system facilitated the breaking of strong hydrogen bonds in lignin and the binding of the aromatic nucleus to the aliphatic chain region, leading to a much higher solubility of lignin.[37] However, the lignin removal efficiency decreased to 46.32% with an increase in the GVL percentage. The cellulose retention decreased from 99.33% to 95.85% when the ratio increased from 1 : 4 : 0 to 1 : 4 : 15. This is attributed to the introduction of excess third-party solvents, where the hydrogen bonding effect was changed.[31] The solvation effect was transformed into a catalytic effect. The ionized H ions in 5Saa attacked the cellulose fraction of lignocellulose. This led to a decrease in lignin solubilization and enhanced cellulose solubilization. Therefore, the optimal ChCl : 5Saa : GVL ratio for ChCl–5Saa/GVL treatment was 1 : 4 : 15.

Temperature has a crucial influence on the mass transfer effect of H protons. Xue *et al.*[37] showed that temperature has a significant effect on the solubility of lignin in various solvents. Therefore, the effect of reaction temperature on lignin removal efficiency was studied at 100 °C, 110 °C, 120 °C, 130 °C, and 140 °C for 2.0 h. The ChCl : 5Saa : GVL ratio was 1 : 4 : 15. Fig. 2b shows that the efficiency of lignin removal increased with increasing temperature. It increased from 44.24% to 84.39% when the reaction temperature was increased from 100 °C to 140 °C. At 120 °C, the lignin removal efficiency, cellulose retention, and solid recovery were 67.23%, 95.82%, and 51.25%, respectively. This indicates that effective lignin disassembly and solubilization were achieved while the integrity of the cellulose bundles was enhanced when the ChCl–5Saa/GVL solvent system was used at 120 °C. However, at 130 °C, the cellulose retention decreased significantly to 78.93% and the solid recovery decreased to 25.34%. This is attributed to the rapid cleavage of hydrogen, ether, and glycosidic bonds in the biomass cell walls under the intense reaction conditions.[15] Lignin, hemicellulose, and cellulose were rapidly removed as the reaction temperature increased. Some lignin groups were modified at high temperatures. The chemical reactions of the

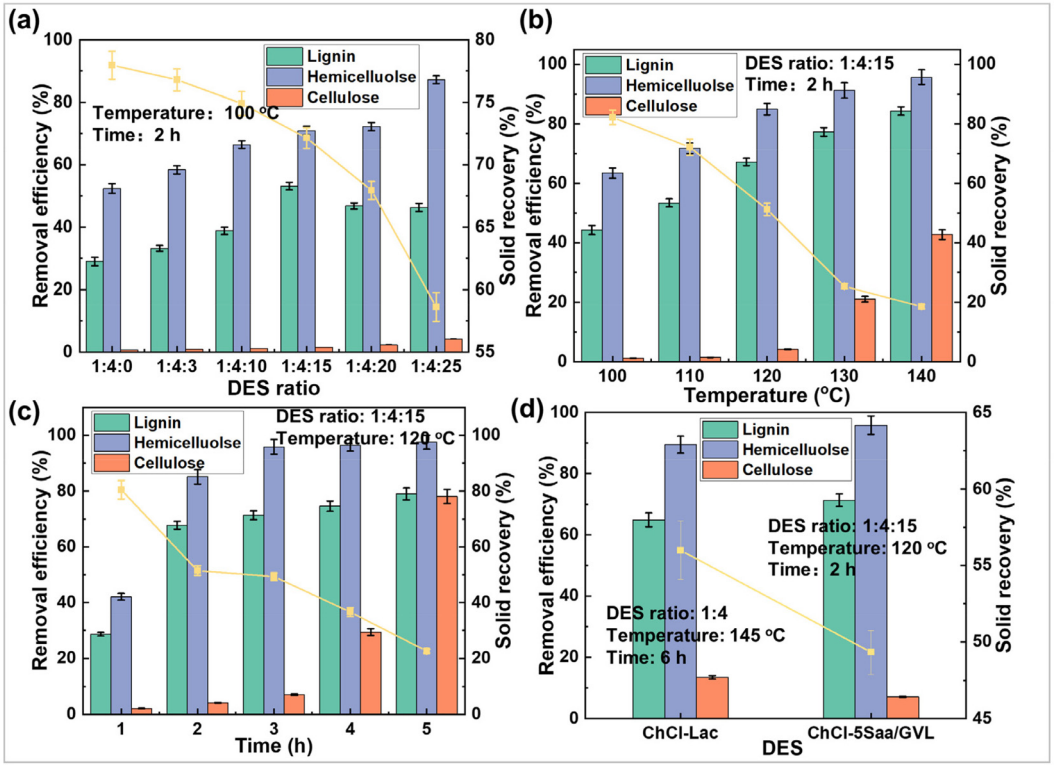

Fig. 2 Separation efficiency of poplar fractions by ChCl–5Saa/GVL treatment ((a) molar ratio of ChCl–5Saa/GVL; (b) temperature; (c) time; (d) extraction rate and purity of lignin under ChCl–Lac and ChCl–5Saa/GVL system treatments).

more active reactive groups were promoted, such as hydroxyl (–OH) and methoxy (–OMe). Therefore, the optimum reaction temperature for ChCl–5Saa/GVL treatment was 120 °C.

Reaction time is an important factor influencing biomass deconstruction. Wang *et al.*[38] showed that a longer reaction time enhanced the dissociation of plant cell walls, allowing the dissociation of lignin macromolecules into small molecular fragments. Therefore, the effect of ChCl–5Saa/GVL treatment on lignin removal and removal efficiency at different reaction times (1, 2, 3, 4, and 5 h) was investigated. The ratio of ChCl : 5Saa : GVL was 1 : 4 : 15, and the reaction temperature was 120 °C. Fig. 2c shows that the lignin removal efficiency increased from 28.63% to 78.99% after 5 h. The lignin and cellulose removal efficiencies were 71.35% and 7.13%, respectively, at 3 h. This indicates that a suitable reaction time not only improves lignin dissolution but also protects the cellulose from excessive destruction. However, the cellulose retention decreased significantly (70.61%) when the reaction time exceeded 3 h. The lignin removal efficiency reached a maximum at 5 h. However, although the lignin removal efficiency was as high as 78.99%, the solid recovery was as low as 22.58%. This indicates that efficient fractionation of lignin and efficient utilization of the remaining lignocellulose fraction cannot be achieved by longer treatment times. Therefore, the optimal reaction time for ChCl–5Saa/GVL treatment was 3.0 h.

In summary, the optimal reaction conditions for the ChCl–5Saa/GVL treatment were as follows: a ChCl : 5Saa : GVL ratio of 1 : 4 : 15, temperature of 120 °C, and reaction time of 3.0 h. The separation efficiencies of lignin, hemicellulose, and cellulose were 71.35%, 95.86%, and 7.13% (92.87% cellulose retention), respectively. Lignin was precipitated by the excess water, and hemicellulose, consisting mainly of xylose (52.6% content), was dissolved in the hydrolysate. At the same time, small amounts of formic acid, acetic acid, furfural and 5-hydroxymethylfurfural were also present in the hydrolyzed solution. Many studies have shown that the ChCl–Lac system has a better effect on the separation of poplar lignin.[26] Therefore, the fractionation effects of the ChCl–5Saa/GVL and ChCl–Lac solvent systems on lignin were compared. Using the ChCl–Lac treatment, the lignin separation efficiency decreased by 6.18% (64.95%), as shown in Fig. 2d. In addition, cellulose structure breakage increased. The cellulose separation efficiency was twice as high (13.51%) under ChCl–Lac treatment. Thus, the fractionation efficiency of lignin was improved by ChCl–5Saa/GVL. In addition, the recycling performance of ChCl–5Saa/GVL was analyzed. The lignin separation was still as high as 68.85% and cellulose retention was 94.02% after 5 cycles (Table S2†). It was still higher than the separation effect of conventional DESs.[20] Therefore, ChCl–5Saa/GVL has excellent recyclability for efficient selective separation of lignin.

Furthermore, this work was compared with the previously reported separation efficiency of the green advanced DES system for lignin (Fig. S1 and Table S1†). First, the sizes of the raw materials were small, concentrated in 0.18–0.85 mm in the

previous DES pretreatments.[19,39,40] In contrast, the wood strips (1.5 × 1.5 × 5 cm) were used directly for the fractionation of lignin in this work. The means that the permeability of ChCl–5Saa/GVL was greatly improved, the separation process was simplified, and the separation energy consumption was reduced compared to previous studies. In addition, the reaction time required to achieve the optimal separation efficiency of lignin was up to 8 h in previous studies. However, it was as low as 3 h at the same temperature with ChCl–5Saa/GVL pretreatment. In particular, the separation efficiency of lignin was 10–30% higher.[41,42] This suggested that the separation efficiency of lignin was substantially improved. Last but not least, only about 7% of the cellulose was removed. This suggested that the high-value utilization of lignin and cellulose fractions had improved.

Changes in the surface morphology and chemical structure of lignocellulose after treatment with ChCl–5Saa/GVL

The fractionation of lignin using the ChCl–5Saa/GVL system was visualized by the structural changes in the wood cell wall. Cross-sectional and chordal sections of poplar wood were observed using SEM before and after the various treatments. Fig. 3 shows lignin autofluorescence images. The cross-sectional structure of virgin poplar (RUW) was highly dense (Fig. 3a). The wooden rays on the surface of the poplar chord section were smooth and intact (Fig. 3d). The intact cellular structure of the poplar cross-section was clearly observed. A large amount of red fluorescence from lignin imaging filled the wood between the cell walls. The fiber bundle walls collapsed and deformed after ChCl–Lac treatment (Fig. 3b). This is due to the removal of large amounts of lignin and hemicellulose. Moreover, the separated lignin formed dense, condensed spherical structures attached to the cell bundle tube walls (Fig. 3e). A large number of condensed spherical lignin particles were observed under CLSM fluorescence (Fig. 3h). The fiber bundle tubes were loosely arranged (Fig. 3c) after ChCl–5Saa/GVL treatment. The surface of the fiber bundle tube wall was smooth and structurally intact (Fig. 3f). However, the lignin fluorescence disappeared. This indicates that a large amount of lignin was removed after treatment with ChCl–5Saa/GVL, which demonstrates good lignin solubilization.

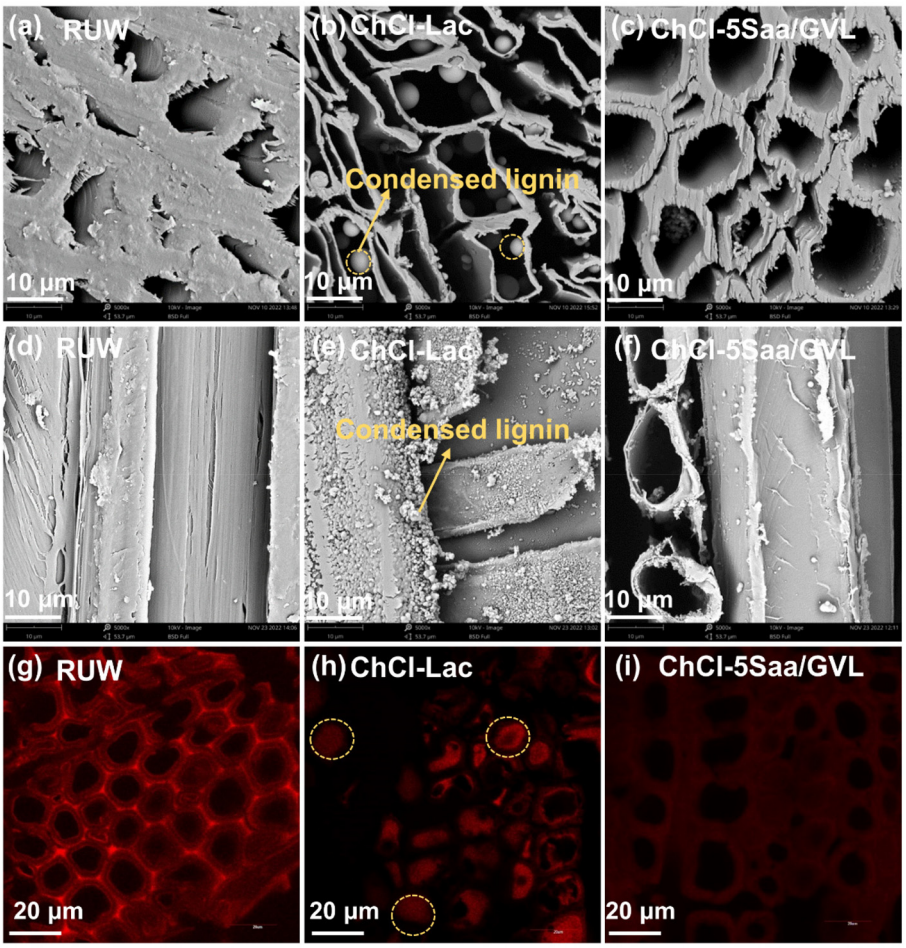

Fig. 3 Changes in the apparent morphology of poplar fibers before and after treatment with different DES systems ((a–c) SEM of different poplar cross-sections; (d–f) SEM of different poplar chordal sections; (g–i) CLSM of different poplar cross-sections).

The cell walls of lignocellulose grew from the outside to the inside, and hemicellulose and lignin acted as adhesives and fillers to tightly bind the intercellular layer and the primary and secondary walls, bonding the adjacent microfiber bundles together (Fig. 3a). The effect of DES on the chemical structure of poplar fibers was analyzed. As shown in Fig. 4a, at 1657 cm^{-1}, the stretching vibration peaks attributed to the carbonyl C═O of the aromatic ring disappeared after treatment. The peaks at 1600 cm^{-1}, 1507 cm^{-1} and 1425 cm^{-1} were attributed to the stretching vibrations of the aromatic ring backbone. The intensities of these absorption peaks significantly weakened after the DES treatment. At 1328 cm^{-1}, the absorption peak attributed to the lilac nucleus disappeared. At 1265 cm^{-1}, the methoxy absorption peak attributed to guaiacol disappeared. The results indicate that the DES treatment had a good decomposition effect on lignin. In addition, at 1158 cm^{-1}, the intensity of the C–O–C stretching vibration peak of the furan ring decreased after the treatment. At 1050 cm^{-1}, the intensity of the stretching vibration absorption peak of the hemicellulose carbonyl C–O decreased. In particular, at 890 cm^{-1}, the C–H bending vibration absorption peak of –D-xylose disappeared after ChCl–5Saa/GVL treatment. This shows that lignin removal was accompanied by hemicellulose decomposition. A significant increase in the relative cellulose content was observed in the residual solid samples with the deconstruction of hemicellulose and lignin. The fiber crystallinity index increased from 58.10% to 70.29% after ChCl–5Saa/GVL treatment (Fig. 4b). This increased the crystallinity index by 3.0% over that of the ChCl–Lac-treated samples. The results showed that ChCl–5Saa/GVL treatment had a significant effect on the deconstruction of lignin and hemicellulose, and residual solids containing higher cellulose content were obtained.

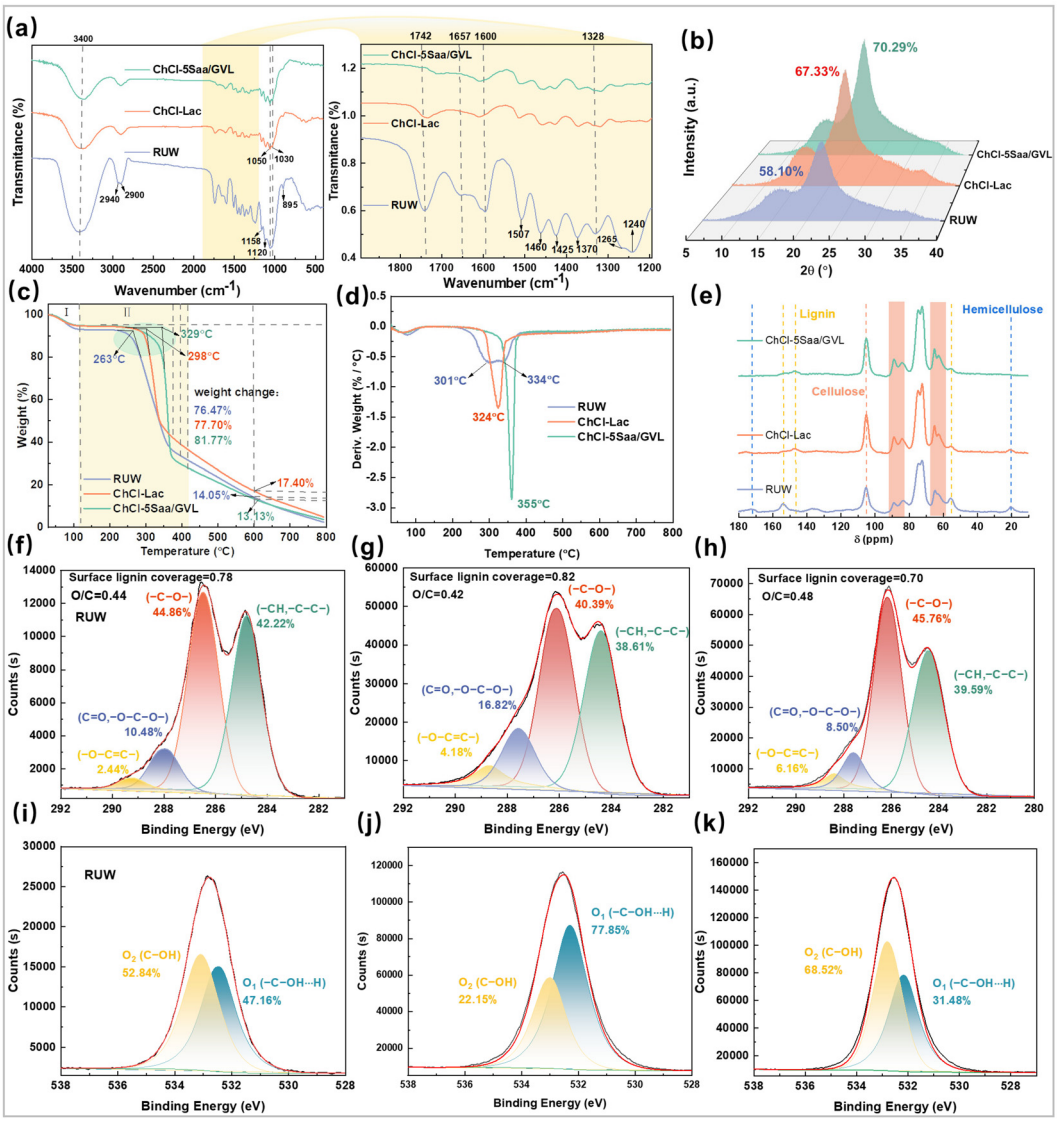

Fig. 4 Changes in the chemical structure of poplar fibers before and after treatment with different DES systems ((a) FTIR; (b) XRD; (c) TGA; (d) DTG; (e) ^{13}C-CP/MAS-NMR; (f–h) elemental carbon peaks of XPS of different poplar fibers; (i–k) elemental oxygen peaks of XPS of different poplar fibers).

The changes in the thermal stability of the poplar wood samples before and after the DES treatment are shown in Fig. 4c and d. First, the initial pyrolysis temperature of the samples increased from 263 °C to 298 °C and 329 °C after DES treatment. The DTG curves show decomposition temperatures of 301 °C and 334 °C at the maximum thermal degradation rate (Fig. 4d). These peaks are attributed to the thermal degradation of hemicellulose and thermal degradation peak of cellulose, respectively. Due to the wide temperature range of thermal degradation of lignin (250–500 °C), no significant peak was observed at the maximum thermal degradation rate of lignin. The residual solids after the ChCl–5Saa/GVL treatment reached the maximum thermal degradation rate at 355 °C, which is higher by 31 °C than that after ChCl–Lac treatment (324 °C). Therefore, the ChCl–5Saa/GVL treatment preserved the high-purity cellulose component while separating lignin.

The structural characteristics of the chemical fraction of the residual poplar solids were investigated before and after treatment with the DES system.[43] Therefore, Fig. 4e shows the peaks at 172 and 20 ppm of carbon atoms attributed to the acetylated C═O and –CH_3 groups of hemicellulose, respectively. The peaks at 153 ppm, 147 ppm, and 55 ppm were attributed to the carbon atoms of the etherified lilac unit (S), guaiacyl unit (G), and –OMe of lignin, respectively. The peaks at 89, 83, 65, and 62 ppm are attributed to the carbon atoms of celluloses C_4 and C_6, respectively. The attribution peaks of lignin were significantly attenuated after DES treatment. In addition, the hemicellulose carbon atom attribution peaks of ChCl–5Saa/GVL completely disappeared, unlike those of ChCl–Lac. Significant double peaks were observed at 62 ppm and 65 ppm. These were attributed to the increased relative content of the crystalline cellulose region. The results show that the ChCl–5Saa/GVL system deconstructs lignin to obtain a high-purity cellulose fraction, which is very effective in the deconstruction of the three major components of poplar wood.

The lignin depolymerization and repolymerization reactions were found to occur simultaneously during the lignin solubilization process.[44] Therefore, the surface elemental content of the samples was analyzed.[45] As shown in Fig. 4f and g, the ChCl–Lac system isolated a large amount of lignin, and the C_1 (–C–C) content of ChCl–Lac increased from 42.22% to 38.61% compared to RUW. However, the lignin surface coverage of ChCl–Lac increased from 0.78 to 0.82. This indicates that a new –C–C structure was produced, which resulted in lignin being deposited on the cellulose surface during lignin deconstruction using ChCl–Lac. This observation is consistent with SEM observations (Fig. 3). In addition, C_1 of ChCl–5Saa/GVL was as low as 39.59% (Fig. 4h). The relative contents of the surface elements of the lignin and aromatic extracts decreased by 2.63%; C_4 increased to 6.16%; and the O/C ratio increased to 0.48. The coverage of the surface lignin was reduced by 0.08 (0.7). These results suggest that the formation of –C–C-linked bonds was hindered during ChCl–5Saa/GVL deconstruction and lignin solubilization.[46] This conclusion was also verified by the fractionation of elemental oxygen (Fig. 4i–k). Therefore, high cellulose surface accessibility was achieved after the ChCl–5Saa/GVL system treatment.

Structural analysis of regenerated lignin

The purity, chemical structure, and active-group content of lignin are crucial for its high-value utilization. Therefore, ChCl–Lac and ChCl–5Saa/GVL fractionated lignin (ChCl–Lac–Lignin and ChCl–5Saa/GVL–Lignin) were analyzed (Fig. S3†). The results are shown in Fig. 5 and Table 1. The ChCl–5Saa/GVL system had a higher lignin separation efficiency and extraction rate than the ChCl–Lac system. These values were 71.35% and 70.35%, respectively. The purity of ChCl–5Saa/GVL–Lignin was 98.77%. The number average molecular weight (M_n) of ChCl–Lac–Lignin and ChCl–5Saa/GVL–Lignin was 2181 g mol^{-1} and 2305 g mol^{-1}, respectively, and the polydispersity values were 2.13 and 1.80, respectively. Therefore, ChCl–5Saa/GVL fractionated lignin fragments with high purity showed better molecular homogeneity.

The β-O-4 aryl ether bond (A), β-β (B), and β-5 (C) were the major linkage bonds and substructures in the side chain region of poplar lignin. The aromatic region was dominated by syringyl (S) and a small amount of guaiacyl (G). The substructures of δ_C/δ_H 71.10/3.82 (B_γ), δ_C/δ_H 71.10/4.20 (B_γ), a small amount of δ_C/δ_H 111.59/6.99 (G_2), and a large amount of δ_C/δ_H 131.99/7.71 (PB) were retained in ChCl–5Saa/GVL–Lignin as compared to the ChCl–Lac–Lignin structure. This is very similar to the original lignin structure. In addition, ChCl–5Saa/GVL–Lignin contained 26% G-units. This is three times the number of G-units in ChCl–Lac–Lignin. The S/G ratios of ChCl–Lac–Lignin and ChCl–5Saa/GVL–Lignin were 9.95 and 2.87, respectively (Table 2). This is attributed to the aggregation of GVL around the lignin fragment molecules and the formation of a protective ring. The G-units of ChCl–5Saa/GVL–Lignin were well-reserved during fractionation. The G-units have a stronger reactivity than the S-units. Therefore, lignin isolated by ChCl–5Saa/GVL has more reactive groups.

ChCl–Lac–Lignin and ChCl–5Saa/GVL–Lignin were analyzed by ^{31}P NMR. The phenolic hydroxyl contents of the different regenerated lignin were compared as shown in Table 3 (Fig. S2†). The higher the phenolic hydroxyl content, the more chemically reactive the lignin.[27] Table 3 shows that the total phenolic hydroxyl content in ChCl–5Saa/GVL–Lignin was as high as 6.92 mmol g^{-1}. This is attributed to the increase in hydroxyl content caused by the breakage of β-O-4 aryl ether bonds and other depolymerization reactions.[19] In addition, ChCl–5Saa/GVL–Lignin contained more aliphatic OH groups and guaiacyl OH groups than ChCl–Lac–Lignin, which were 2.67 mmol g^{-1} and 2.03 mmol g^{-1}, respectively. This suggests that the fractionated lignin from the ChCl–5Saa/GVL system is a polyphenolic lignin that retains more G-units with high reactivity. Therefore, the ChCl–5Saa/GVL solvent system was able to extract lignin with high yield, high purity, and a large number of active sites.

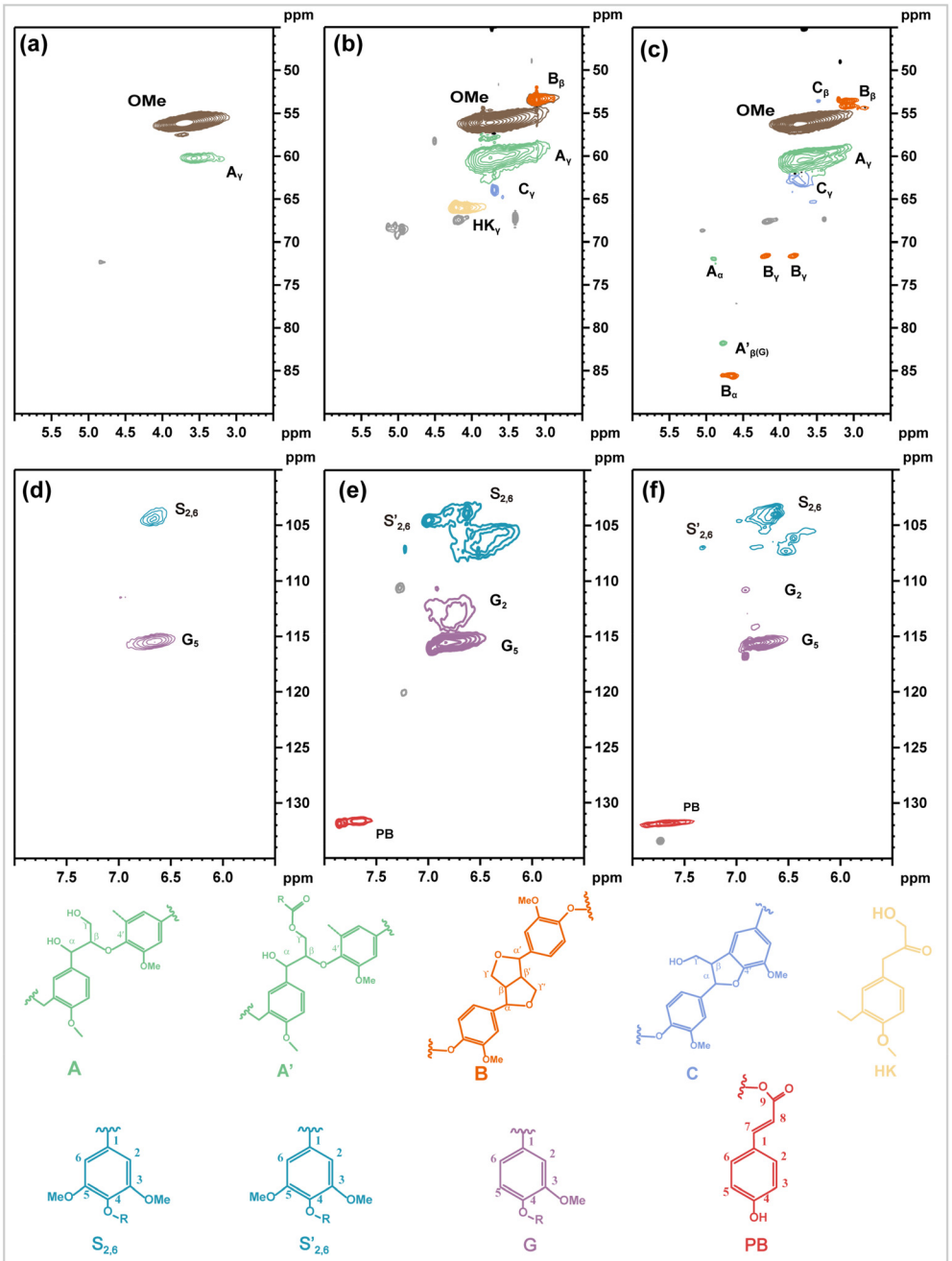

Fig. 5 2D-HSQC of regenerated lignin treated with different DES systems ((a and d) alkali lignin; (b and e) ChCl–Lac–Lignin; (c and f) ChCl–5Saa/GVL–Lignin).

Table 1 Purity and molecular weight of lignin

	M_n (g mol^{-1})	M_w (g mol^{-1})	M_w/M_n	Separation efficiency (%)	Extraction yield (%)	Purity (%)
CEL	3072	4822	1.57	—	—	—
Alkali lignin	2582	3656	2.32	—	—	—
ChCl–Lac	2181	4648	2.13	64.93	63.46	94.85
ChCl–5Saa/GVL	2305	4162	1.80	71.35	70.35	98.77

M_n: the number average molecular weight; M_w: the heavy average molecular weight; M_w/M_n: polydispersity.

Table 2 Structural features (aromatic units, S/G ratio, and lignin unit interconnection) of the integrated lignin samples determined by 2D-HSQC NMR

	S (%)	G (%)	S/G	β-O-4 (%)	β-β (%)	β-5 (%)
CEL	56	44	1.27	61	9	4
ChCl–Lac	79	21	3.85	—	—	—
ChCl–5Saa/GVL	84	16	5.35	—	—	—
ChCl–Lac–Lignin	91	9	9.95	—	—	—
ChCl–5Saa/GVL–Lignin	74	26	2.87	—	—	—

Structural analysis of lignin in residual solids

The lignin solubilization mechanism of ChCl–5Saa/GVL solvent was investigated. In addition, the reasons for the increased phenolic hydroxyl content and the high retention of G-units structures were investigated. The hydrocarbon functional groups of poplar lignin were determined before and after the various treatments in Fig. 6 (Fig. S4†). CEL was the original lignin extracted from untreated poplar wood. Its structure was recognized as the original structure of lignin. Structural changes in the lignin in the residual solids were identified by comparison with the CEL. Fig. 6 shows that the lignin side chain region contains –OMe, A_γ, and B_β after the ChCl–Lac treatment. This indicates that the β ether bond in lignin was severed. In addition, a strong signal peak was observed at δ_C/δ_H 66.50/4.23, which is attributed to the C_γ substructure of the Hibbert ketone (HK). This indicates that monoketone and diketone structures were generated during the ChCl–Lac deconstruction of lignin. G_5 and a small number of $S_{2,6}$ structures were observed in the aromatic region. The signal from the G_6 unit disappeared. The signal of the G_2 unit was diminished, and the signal peak shifted from δ_C/δ_H 111.42/6.99 to δ_C/δ_H 113.34/6.78. This indicates that the G-unit structures were preferentially degraded. Numerous unknown structures were found in ChCl–Lac at δ_C/δ_H 106.70/6.44 and δ_C/δ_H 113.50/6.75, which reveals that the position of the aromatic unit ($S_{2.6}$, G_6, G_2) had changed significantly during the ChCl–Lac treatment.

The residual lignin structure was similar to that of the CEL structure after ChCl–5Saa/GVL treatment. The δ_C/δ_H 62.97/3.74 (C_γ) and δ_C/δ_H 71.10/4.20 (B_γ) substructures were retained. The total phenolic hydroxyl content increased to 6.22 mmol g^{-1} (Table 2). This was three times higher than that of CEL and is attributed to the cleavage of β-O-4 after treatment with the DES solution. The δ_C/δ_H 60.64/3.60 signal at δ_C/δ_H 60.64/3.60 corresponded to the γ position (A_γ) of the side chain of the β-O-4 chain. This implies that an acylation reaction occurred between the –OH group in the lignin substructure and the –COOH in 5Saa.[15] This result is consistent with the findings of previous studies.[19] In addition, the signals δ_C/δ_H 72.39/4.88 for the α-position (A_α) and δ_C/δ_H 84.1/4.4 and δ_C/δ_H 86.5/4.07 for the β-position (A_β) attributed to the side chains of the β-O-4 chain were not detected. This suggests that α and β sites of the A structure were selectively cut off during β-O-4 cleavage. The attribution signals δ_C/δ_H 84.98/4.75 for the α-position B_α, δ_C/δ_H 87.45/5.49 for the α-position C_α, and δ_C/δ_H 53.20/3.56 for the β-position C_β of the β-β chain side chain were not detected. In particular, an unknown structure was found in the aromatic region δ_C/δ_H 106.14/6.61, but small amounts of G_2 and G_6 unit structures were also present. This is attributed to the fact that any new aromatic linkage results in H deficiency at the 2 and 6 positions. However, GVL had timely and effectively solubilized lignin in the ChCl–5Saa/GVL system. Further hydrolysis of lignin molecules in the residual solids was prevented. This was the main reason for the presence of small amounts of unhydrolyzed G_2 and G_6 unit structures.

The lignin in the residual solid of the ChCl–5Saa/GVL system had a higher carboxyl content. This value was three times higher than that in the ChCl–Lac system (Table 3). This indicates that the ester bond was severed during the ChCl–5Saa/GVL fractionation of lignin. In addition, the aliphatic hydroxyl content was three times higher than the residual lignin aliphatic hydroxyls after ChCl–Lac treatment (0.62 mmol g^{-1}). It was 3.41 mmol g^{-1}. This is attributed to the β-O-4 bond breakage and rapid dehydration during condensation in the DES treatment. However, a significant number of reactive oxygen functional groups were retained in the presence of GVL. The S-units and G-units produced by lignin cleavage were solubilized by GVL.[37,47] This indicates that lignin mainly underwent acylation and depolymerization reactions during treatment with the ChCl–5Saa/GVL solvent system. It mainly cut the side chain groups and selectively cut α and β sites of the β-O-4 bond. In particular, both the regenerated lignin obtained from that dissolved in the ChCl–5Saa/GVL solvent system and the lignin in the residual solid retained a lot of the active hydroxyl structure.

Mechanism of fractionation of lignin by ChCl–5Saa/GVL

Lignin solubilization in a ChCl–5Saa/GVL solvent system is crucial for the subsequent high-value utilization of lignin.[48] Therefore, the fractionation mechanisms of lignin using the

Table 3 Hydroxyl content of functional groups in lignin samples quantified by ^{31}P NMR

	CEL	Alkali lignin	ChCl–Lac	ChCl–5Saa/GVL	ChCl–Lac–Lignin	ChCl–5Saa/GVL–Lignin
Aliphatic OH	6.17	1.93	0.62	3.14	1.26	2.67
Carboxylic acid OH	0.15	0.97	0.29	0.30	0.32	0.37
Syringyl OH	0.23	1.49	2.87	3.79	2.17	4.18
Guaiacyl OH	0.86	0.73	1.17	1.78	1.37	2.03
p-Hydroxyphenyl OH	1.05	0.74	0.21	0.66	0.27	0.71
Phenolic OH	2.14	2.96	4.25	6.22	4.35	6.92

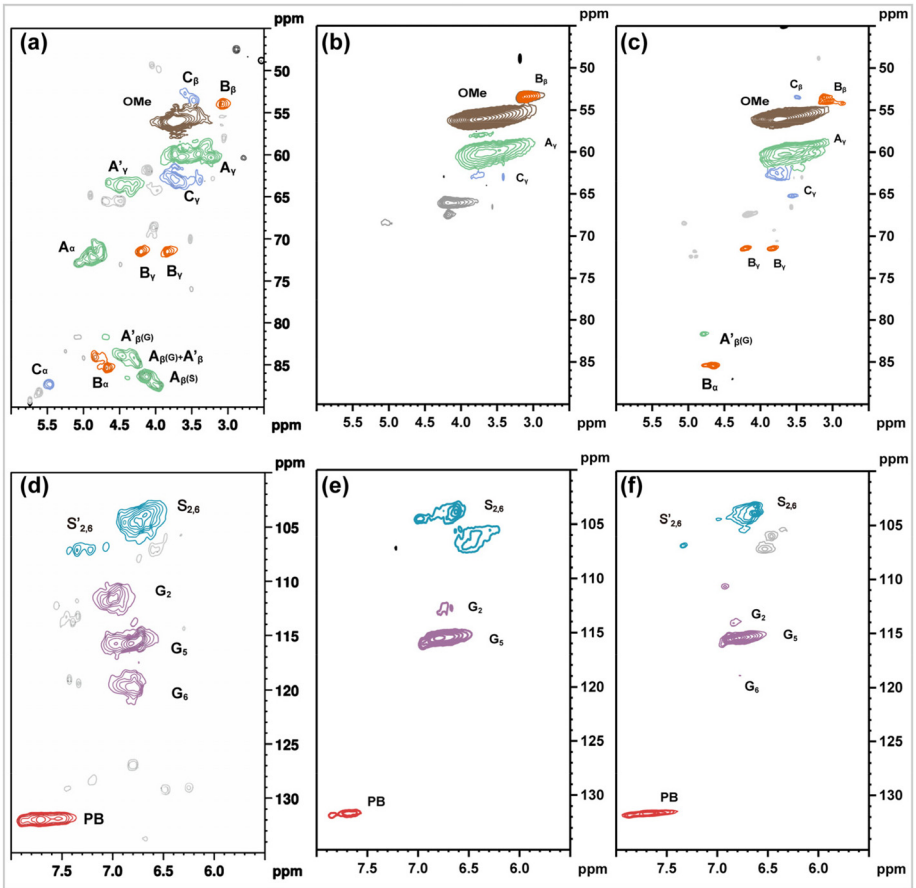

Fig. 6 2D-HSQC of residual lignin in poplar before and after DES treatment ((a and d) CEL; (b and e) residual lignin after ChCl–Lac treatment; (c and f) residual lignin after ChCl–5Saa/GVL treatment).

ChCl–5Saa/GVL solvent system were investigated (Fig. 7). The ester bond between lignin and hemicellulose was preferentially broken owing to the strong hydrogen-bonding network structure within ChCl–5Saa[49] (Fig. 7a). Then, the β-O-4 bond between lignin molecules was severed[22] and small lignin fragments (M_n = 2305 g mol^{-1}) were formed (Fig. 7b). In addition, reactive intermediates were formed along with the cleavage of β-O-4 bonds. These intermediates undergo coupling to form C–C bonds with a high bonding energy.[50] However, 2D-HSQC NMR analysis showed that β-5 and β-β structures did not appear in ChCl–5Saa/GVL–Lignin. The phenolic hydroxyl content increased to 6.92 mmol g^{-1}. This indicates that the carbo-positive active intermediates generated during the reaction were stable. In fact, the GVL molecular structure contains heteroatom oxygen (O), which has a conjugation effect between the lone pair of electrons and the central carbon and thus improves the stability of the carbon-positive ion.[51,52] This is the essence of the regulation of lignin molecular structure in a ChCl–5Saa/GVL solvent system treatment.

Performance analysis of highly reactive LNPs

The particle size, homogeneity and reactivity of LPNs are closely related to the structure and molecular weight of lignin. In particular, the availability of lignin extracted by using the ChCl–5Saa/GVL system was verified. CEL, alkali lignin, ChCl–Lac–Lignin and ChCl–5Saa/GVL–Lignin were used to prepare LNPs, which were named CEL-NP, AL-NP, CLL-NP and CSGL-NP, respectively. The structural and property analysis of different types of LNPs is shown in Fig. 8. LNPs were prepared by an anti-solvent method.[53] With the introduction of water, the hydrophobic structure of lignin (benzene ring, side chain structure) was driven by π–π interactions to aggregate inward to reduce the surface tension.[54] Spherical particles were formed by the inward aggregation of hydrophobic groups and the outward orientation of hydrophilic groups (–OH, –COOH) (Fig. 8a and d). The particle size analysis of the LNPs revealed that the particle sizes of CLL-NP and CSGL-NP were smaller than 100 nm. It was clear that nanoscale lignin (33 nm and 23 nm) was obtained using the DES system after treatment. The CSGL-NP was found to have good homogeneity and dispersion (Fig. 8b). The correlation between LNP size and lignin structure was analyzed. It was shown that the size of LNPs decreased with the molecular weight of lignin. In fact, lignin of different molecular weights could be extracted by the modulation of the ChCl–5Saa/GVL system. The directional modulation of the LNP size was achieved. Furthermore, the particle

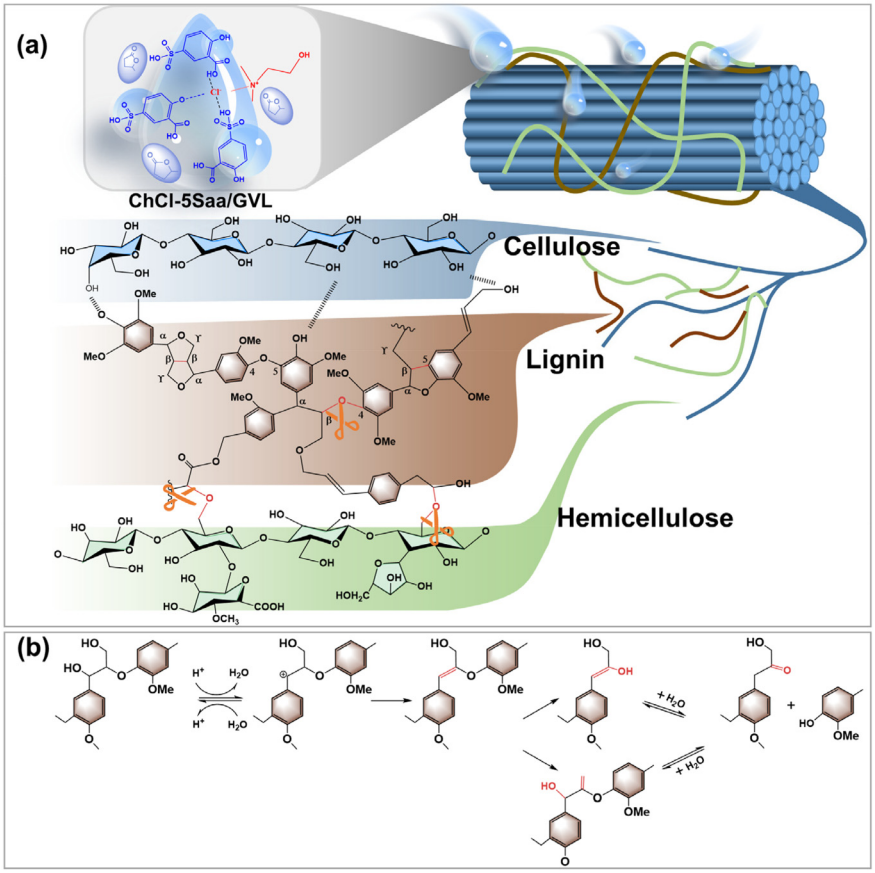

Fig. 7 Schematic of the fractionation mechanism of lignin by ChCl–5Saa/GVL ((a) deconstruction pathway of the linkage bonds between poplar components; (b) reaction pathway of lignin during deconstruction).

dispersion stability of CEL-NP, AL-NP, and CLL-NP was −12 mV, −16 mV, and −17 mV, respectively, in a neutral environment (pH = 7). In contrast, CSGL-NP was highly stable. It has ζ-potential up to −21 mV. This indicated that the CSGL-NP particles were fine and stable. Numerous reactive functional groups (–OH and –COOH) were present in the molecular structure of ChCl–5Saa/GVL–Lignin in ^{31}P NMR results. Therefore, LNPs have higher chemical reactivity. And the electrostatic repulsive effect between the particles kept the colloidal particles highly stable.[54,55] This meant that LNPs with a high ζ-potential could be used as a flocculant.[56] Polar organic matter in water was adsorbed using electrostatic interaction and hydrogen bonding of LNPs. Flocculation and sedimentation of suspended particles was achieved.

UV resistance was one of the properties of lignin products.[57] The transmittance of CEL-NP, AL-NP, and CLL-NP is 0%. This indicated that the LNPs have good UV resistance in the wavelength range of 200–400 nm, as shown in Fig. 8e. In comparison, AL-NP had a high transmittance. Its transmittance increased rapidly from 320 nm wavelength after. It was 30%. CSGL-NP has better UV shielding performance compared to alkali lignin. This was attributed to the small amount of –OMe and A_γ structures in the side chain of alkali lignin. The G_5-unit structure was retained in the aromatic region. The rest of the structures were degraded (Fig. 5a and d). In contrast, the ChCl–5Saa/GVL–Lignin contained a large number of chromogenic groups (benzene ring, carbonyl group, double bond) and color-assisting groups (phenolic hydroxyl group, –OMe). In addition, more G-units were retained. Lignin was endowed with stronger reactivity. UV-induced radicals were effectively captured using phenolic hydroxyl groups. The oxidative damage caused by UV radiation was mitigated.[58] Aging of the material was inhibited due to effective scavenging of free radicals.[59] The results showed that high quality high purity lignin was fractionated using the ChCl–5Saa/GVL solvent system compared to alkali lignin and CEL. LNPs with high stability, homogeneity and high activity were prepared using this small molecular weight of highly active lignin. This opened up new possibilities for the development of high-end lignin-based materials.

Materials and methods

Materials

A 12-year-old poplar was obtained from the Henan Forest Farm (Zhengzhou, China). The cellulose, hemicellulose, and lignin contents were analyzed using an acid digestion method devel-

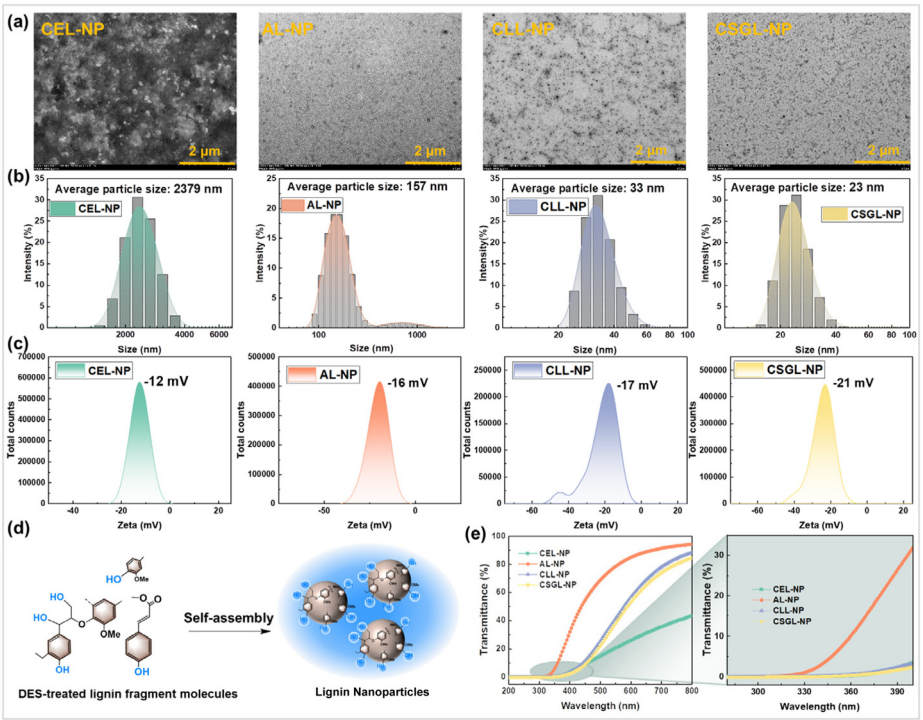

Fig. 8 LNPs prepared from different types of lignin ((a) TEM; (b) particle size; (c) ζ-potential; (d) formation mechanism of LNPs; (e) UV shielding properties).

oped by the National Renewable Energy Laboratory (NREL, USA).[24] The contents were 43.16%, 16.04%, and 29.82%, respectively. ChCl, 5Saa, GVL, lactic acid (Lac), alkali lignin and other reagents were purchased from Aladdin (Shanghai, China).

Preparation of ChCl–5Saa/GVL

Choline chloride and 5-sulfosalicylic acid were mixed in a water bath in a molar ratio of 1 : 4. The homogeneous and clear mixture was removed at 80 °C and 150 rpm after 90 min of reaction. The resulting mixture was denoted as ChCl–5Saa. A solution of GVL was added to the prepared ChCl–5Saa at a certain concentration. A new DES system (ChCl–5Saa/GVL) was obtained by stirring the mixture well. The ChCl–5Saa/GVL solution was then cooled to room temperature without crystallization. The samples were stored in a desiccator to prevent moisture absorption. In addition, the properties of different deep eutectic solvent systems were compared and analyzed. A ChCl–lactic acid (ChCl–Lac) solution was prepared according to the method in the literature.[60]

Characterization of ChCl–5Saa/GVL

First, the density of the DES was determined using the weight method. The melting point of the DES was detected by differential scanning calorimetry (DSC 25, TA Instruments, New York, Delaware, USA). Temperature range was 30–100 °C. The conductivity was determined using a conductivity meter (DDS-307A, Precision Scientific, Shanghai, China). Viscosity was analyzed using a rotational rheometer (HR 20, TA Instruments-Waters LLC, New York, Delaware, USA). The hydrogen bonding composition of the DES was analyzed using Fourier infrared spectroscopy (FTIR, TENSOR27, Bruker, Neckarsulm, Germany) and nuclear magnetic resonance spectroscopy (NMR, AVANCE III HD 500M, Bruker, Neckarsulm, Germany). Details of the procedures were described by Parra and his collaborators.[61]

The molecular properties of the DES solvents were analyzed by determining the Kamlet–Taft (K–T) parameters. The specific analysis method was described by Hong and co-workers.[19] Nile red (NR), 4-nitroaniline (NA), and *N*,*N*-diethyl-4-nitroaniline (DENA) were dissolved in methanol. The concentrations were all 1.0 mg mL^{-1}. 0.5 mL of NR, NA, and DENA were placed in separate centrifuge tubes. Next, 3 mL of DES solution was added, sonicated, and mixed at 25 °C. The maximum absorption wavelength of the solutions at 250–800 nm was determined using a UV spectrophotometer (CARY 3500 UV-VIS; Agilent, Santa Clara, CA, USA).

Fractionation of lignin from poplar wood

Poplar wood strips (1.5 × 1.5 × 5 cm) were mixed with DES solvent systems (ChCl–5Saa and ChCl–5Saa/GVL) at a solid–liquid ratio of 1 : 10. Lignin fractionation was performed in a high-temperature oven (FDL 115, Binder, Neckarsulm, Germany). The residual solids collected at the end of the reaction were washed to a neutral pH using distilled water. Then, samples were washed using THF to remove reprecipitation of

lignin. Finally, it was stored in a sealed container after drying at 45 °C after ultrapure water washing. Lignin was precipitated from the filtrate by adding distilled water to the filtrate. The specific procedure for determining the content of the three main components of poplar wood (cellulose, hemicellulose and lignin) is to firstly subject poplar wood to acidolytic treatment. The main components of poplar wood are converted into small molecules of monosaccharides. Then, the monosaccharide content was determined using gel permeation chromatography (GPC, AGILENT 1260 Infinity II, Agilent, Santa Clara, CA, USA). The lignin content was calculated as the sum of acid-soluble lignin and precipitated lignin. Acid-soluble lignin content was determined using a UV spectrophotometer (CARY 3500 UV-VIS; Agilent Technologies, Santa Clara, CA, USA). The precipitated lignin content was analyzed using the weight method.[62] In addition, the preparation process for the comparison samples was as follows. 1.5 × 1.5 × 5 cm poplar wood strips were mixed with ChCl–Lac, where the molar ratio of ChCl–Lac was 1 : 4 and the solid–liquid ratio was 1 : 10. The reaction was carried out in a high-temperature reactor at 145 °C for 6 h.[26]

Physicochemical properties of residual solid

The apparent morphology and internal component distribution of the different poplar samples were characterized using scanning electron microscopy (SEM, SU8220, Hitachi, Tokyo, Japan) and confocal laser scanning microscopy (CLSM, FV10i, Olympus Corporation, Tokyo, Japan). The effects of DES treatment on the thermal stability and crystallinity index of the fibers were analyzed using a thermogravimetric analyzer (TGA, TGA55, TA Instruments, New York, Delaware, USA) and an X-ray diffractometer (XRD, MINFLEX600, Rigaku Corporation, Tokyo, Japan). The patterns of variation in the main structural features of the different components of poplar wood were analyzed using Fourier-transform infrared spectroscopy (FTIR, TENSOR27, Bruker, Karlsruhe, Germany), X-ray photoelectron spectroscopy (XPS, Thermo Fisher Scientific, ESCALAB 250XI$^+$, Waltham, MA, USA), and 13-carbon nuclear magnetic resonance (^{13}C-CP/MAS-NMR, AVANCE NEO 400WB, Bruker, Karlsruhe, Germany). Details of procedures and instruments were described by Liu and his collaborators.[63]

Characterization of regenerated lignin and residual solid lignin

Lignin was isolated from poplar wood by cellulase hydrolysis (CEL). The extraction method is in agreement with that reported by Wu and co-workers.[64] The effect of DES treatment on the structure of the residual lignin in poplar was analyzed. In addition, the structure of the DES-fractionated lignin was analyzed. The unit structures of the residual and fractionated lignin samples were characterized by 2D-HSQC NMR (AVANCE III HD 500M, Bruker, Karlsruhe, Germany). 60 mg of lignin was allowed to dissolve in dimethyl sulfoxide-d_6 (DMSO-d_6) for assay analysis. Detailed steps can be found in previous studies.[19] (The detailed calculation of the quantification of lignin inter-unit linkages is given in the ESI.†) The structural unit ratios and hydroxyl contents were quantified using ^{31}P NMR. Detailed steps can be found in previous studies.[65] The molecular weights of the fractionated lignin samples were analyzed by gel permeation chromatography (GPC 50, Agilent, Santa Clara, CA, USA).[63] (The detailed calculation of the quantification of OH groups is given in the ESI.†)

Preparation and characterization of LNPs

2.0 mg mL^{-1} lignin was dissolved in tetrahydrofuran (THF). A lignin master batch was prepared. Lignin mother liquor at a concentration of 1.0 mL was added to 10 mL of deionized water and stirred at 500 rpm for 10 min. Lignin nanoparticles (LNPs) were obtained after 24 h of freeze-drying.[66] Its apparent morphology was analyzed by transmission electron microscopy (TEM, Advanced Microscope Techniques Corp., Hitachi HT7700, Tokyo, Japan). LNP particle size and zeta (ζ) potential were analyzed using a nanoparticle sizer (Zetasizer Lab, NANO ZS90, London, England). The dispersant is deionized water. The UV-shielding properties were studied using a UV spectrophotometer (CARY 3500 UV-VIS, Agilent, Santa Clara, CA, USA). LNP transmittance was detected at 200–800 nm. The detection method was referred from previous studies.[67]

Conclusions

A deep eutectic solvent for lignin synthesis consisting of ChCl/5Saa and GVL was proposed. Pre-crushing processing of raw materials was avoided due to the new DES solution having stronger permeability compared to the previous DES solutions. The breakage of β-O-4 in lignin was effectively controlled by regulating the relative ratios of the new ternary DES components. High-purity polyphenolic lignin and a more intact cellulose fraction were obtained. Owing to the conjugation effect between the lone pair of electrons on the oxygen heteroatom in GVL and the central carbon atom, the stability of the carbo-positive active intermediates improved. In addition, LNPs with high dispersion stability and excellent UV shielding properties were prepared. In conclusion, this system can replace corrosive, strongly acidic, and conventional organic solvents by combining an acid catalyst and a stabilizer in the DES, thus preparing a new solvent system that is recyclable, non-toxic, and specific for lignin depolymerization and fractionation of biomass. The green advancement of the new DES has been significantly improved. This opens up new possibilities for the development of high-end lignin-based materials.

Author contributions

Conceptualization and writing – review and editing: M. Y.; investigation and writing – original draft: B. L. and L. Q.; funding acquisition and resources: C. Q.; validation: Z. D. and Z. W.; formal analysis: C. H., and C. L.; project administration and supervision: S. Y.

Conflicts of interest

There are no conflicts to declare.

Acknowledgements

This project was sponsored by the National Key Research and Development Program (2022YFC2105505). This project was supported by the Guangxi Natural Science Foundation of China (2023GXNSFGA026001).

Notes and references

1 C. Chio, M. Sain and W. Qin, *Renewable Sustainable Energy Rev.*, 2019, **107**, 232–249.
2 Z.-H. Liu, B.-Z. Li, J. S. Yuan and Y.-J. Yuan, *Trends Biotechnol.*, 2022, **40**, 1550–1566.
3 W. Zhang, X. Chen, J. Zhao, X. Wang, X. Li, T. Liu, B. Luo, Y. Qin, S. Zhang, M. Chi, S. Wang and S. Nie, *Nano Energy*, 2023, **108**, 108196.
4 B. L. Tardy, E. Lizundia, C. Guizani, M. Hakkarainen and M. H. Sipponen, *Mater. Today*, 2023, **65**, 122–132.
5 F. Cheng, S. Liu, S. D. Karlen, H. Kim, F. Lu, J. Ralph, L. M. V. Ramos, G. W. Huber and J. A. Dumesic, *Green Chem.*, 2023, **25**, 336–347.
6 S. Hong, X.-J. Shen, Z. Xue, Z. Sun and T.-Q. Yuan, *Green Chem.*, 2020, **22**, 7219–7232.
7 S. Zhang, M. Chi, J. Mo, T. Liu, Y. Liu, Q. Fu, J. Wang, B. Luo, Y. Qin, S. Wang and S. Nie, *Nat. Commun.*, 2022, **13**, 4168.
8 T. Renders, S. Van den Bosch, S. F. Koelewijn, W. Schutyser and B. F. Sels, *Energy Environ. Sci.*, 2017, **10**, 1551–1557.
9 L. Niu, X. Li, Y. Zhang, H. Yang, J. Feng and Z. Liu, *ACS Sustainable Chem. Eng.*, 2022, **10**, 13081–13090.
10 S. Wang, B. Liu, J. Liang, F. Wang, Y. Bao, C. Qin, C. Liang, C. Huang and S. Yao, *Bioresour. Technol.*, 2023, **382**, 129154.
11 M. Wang and F. Wang, *Adv. Mater.*, 2019, **31**, 1901866.
12 H. Huang, Z. Li, Y. Ma, M. Yao, S. Yao, Z. Zhang and C. Qin, *Carbohydr. Polym.*, 2023, **303**, 120461.
13 C. Feng, J. Zhu, Y. Hou, C. Qin, W. Chen, Y. Nong, Z. Liao, C. Liang, H. Bian and S. Yao, *Bioresour. Technol.*, 2022, **348**, 126793.
14 J. Y. Cheng, C. Huang, Y. N. Zhan, S. M. Han, J. Wang, X. Z. Meng, C. G. Yoo, G. G. Fang and A. J. Ragauskas, *Chem. Eng. J.*, 2022, **443**, 136395.
15 X. J. Shen, T. Y. Chen, H. M. Wang, Q. Q. Mei, F. X. Yue, S. N. Sun, J. L. Wen, T. Q. Yuan and R. C. Sun, *ACS Sustainable Chem. Eng.*, 2020, **8**, 2130–2137.
16 H. Jia and P. Lv, *Green Chem.*, 2020, **22**, 1378–1387.
17 J. Cheng, C. Huang, Y. Zhan, X. Liu, J. Wang, X. Meng, C. G. Yoo, G. Fang and A. J. J. Ragauskas, *Green Chem.*, 2023, **25**, 1571–1581.
18 Z. Gong and L. Shuai, *Trends Chem.*, 2023, **5**, 163–166.
19 S. Hong, X.-J. Shen, B. Pang, Z. Xue, X.-F. Cao, J.-L. Wen, Z.-H. Sun, S. S. Lam, T.-Q. Yuan and R.-C. Sun, *Green Chem.*, 2020, **22**, 1851–1858.
20 Y. T. Tan, G. C. Ngoh and A. S. M. Chua, *Bioresour. Technol.*, 2019, **281**, 359–366.
21 B. Deng, Y. Hou, F. Wang, Y. Bao, F. Zeng, C. Qin, C. Liang, C. Huang, J. Ma and S. Yao, *Bioresour. Technol.*, 2022, **355**, 127304.
22 M. Zhou, O. A. Fakayode, A. E. A. Yagoub, Q. Ji and C. Zhou, *Renewable Sustainable Energy Rev.*, 2022, **156**, 111986.
23 L. Shuai, M. T. Amiri, Y. M. Questell-Santiago, F. Héroguel, Y. Li, H. Kim, R. Meilan, C. Chapple, J. Ralph and J. S. Luterbacher, *Science*, 2016, **354**, 329–333.
24 J. Li, B. Liu, L. Liu, Y. Luo, F. Zeng, C. Qin, C. Liang, C. Huang and S. Yao, *Bioresour. Technol.*, 2023, **376**, 128855.
25 J. S. Luterbacher, A. Azarpira, A. H. Motagamwala, F. Lu, J. Ralph and J. A. Dumesic, *Energy Environ. Sci.*, 2015, **8**, 2657–2663.
26 D. Tian, Y. Guo, J. Hu, G. Yang, J. Zhang, L. Luo, Y. Xiao, S. Deng, D. Deng, W. Zhou and F. Shen, *Int. J. Biol. Macromol.*, 2020, **142**, 288–297.
27 Q. Xia, Y. Liu, J. Meng, W. Cheng, W. Chen, S. Liu, Y. Liu, J. Li and H. Yu, *Green Chem.*, 2018, **20**, 2711–2721.
28 Y. Chen, W. Chen, L. Fu, Y. Yang, Y. Wang, X. Hu, F. Wang and T. Mu, *Ind. Eng. Chem. Res.*, 2019, **58**, 12741–12750.
29 H. T. Yu, Z. M. Xue, R. F. Shi, F. Y. Zhou and T. C. Mu, *Ind. Crops Prod.*, 2022, **184**, 115049.
30 M. Francisco, A. van den Bruinhorst and M. C. Kroon, *Angew. Chem., Int. Ed.*, 2013, **52**, 3074–3085.
31 L. Sapir and D. Harries, *J. Chem. Theory Comput.*, 2020, **16**, 3335–3342.
32 A. P. Abbott, G. Capper, D. L. Davies, R. K. Rasheed and V. Tambyrajah, *Chem. Commun.*, 2003, 70–71.
33 P. G. Jessop, D. A. Jessop, D. Fu and P. Lam, *Green Chem.*, 2012, **14**, 1245–1259.
34 Z. Chen, X. Bai, A. Lusi and C. Wan, *ACS Sustainable Chem. Eng.*, 2018, **6**, 12205–12216.
35 M. Francisco, A. van den Bruinhorst and M. C. Kroon, *Green Chem.*, 2012, **14**, 2153–2157.
36 M. A. Mellmer, D. M. Alonso, J. S. Luterbacher, J. M. R. Gallo and J. A. Dumesic, *Green Chem.*, 2014, **16**, 4659–4662.
37 Z. Xue, X. Zhao, R.-c. Sun and T. Mu, *ACS Sustainable Chem. Eng.*, 2016, **4**, 3864–3870.
38 Z.-K. Wang, S. Hong, J.-l. Wen, C.-y. Ma, L. Tang, H. Jiang, J.-J. Chen, S. Li, X.-J. Shen and T.-Q. Yuan, *ACS Sustainable Chem. Eng.*, 2020, **8**, 1050–1057.
39 Y. Su, C. Huang, C. Lai and Q. Yong, *Bioresour. Technol.*, 2021, **321**, 124471.
40 C. Alvarez-Vasco, R. Ma, M. Quintero, M. Guo, S. Geleynse, K. K. Ramasamy, M. Wolcott and X. Zhang, *Green Chem.*, 2016, **18**, 5133–5141.
41 Y. Liu, W. Chen, Q. Xia, B. Guo, Q. Wang, S. Liu, Y. Liu, J. Li and H. Yu, *ChemSusChem*, 2017, **10**, 1692–1700.

42 Y. T. Tan, A. S. M. Chua and G. C. Ngoh, *Ind. Crops Prod.*, 2020, **154**, 112729.
43 M. Talebi Amiri, G. R. Dick, Y. M. Questell-Santiago and J. S. Luterbacher, *Nat. Protoc.*, 2019, **14**, 921–954.
44 V. Patil, S. Adhikari, P. Cross and H. Jahromi, *Renewable Sustainable Energy Rev.*, 2020, **133**, 110359.
45 Q. Chu, W. Tong, S. Wu, Y. Jin, J. Hu and K. Song, *Green Chem.*, 2021, **23**, 4074–4086.
46 F. Cheng, S. Liu, S. D. Karlen, H. Kim, F. Lu, J. Ralph, L. M. Vázquez Ramos, G. W. Huber and J. A. Dumesic, *Green Chem.*, 2023, **25**, 336–347.
47 J. S. Luterbacher, J. M. Rand, D. M. Alonso, J. Han, J. T. Youngquist, C. T. Maravelias, B. F. Pfleger and J. A. Dumesic, *Science*, 2014, **343**, 277–280.
48 X. Yin, T. Cai, C. Liu, C. Huang, J. Wang, J. Hu, N. Li, J. Jiang and K. Wang, *Chem. Eng. J.*, 2022, **437**, 135408.
49 Y. Liu, N. Deak, Z. Wang, H. Yu, L. Hameleers, E. Jurak, P. J. Deuss and K. Barta, *Nat. Commun.*, 2021, **12**, 5424.
50 L. Shuai, M. T. Amiri, Y. M. Questell-Santiago, F. Heroguel, Y. Li, H. Kim, R. Meilan, C. Chapple, J. Ralph and J. S. Luterbacher, *Science*, 2016, **354**, 329–333.
51 F. P. Lossing and J. L. Holmes, *Chem. Informationsdienst*, 1985, **16**, 10145.
52 P. Cozzi and F. Benfatti, *Angew. Chem., Int. Ed.*, 2010, **49**, 256–259.
53 Y. Ma, Y. Liao, Z. Jiang, Q. Sun, X. Guo, W. Zhang, C. Hu, R. Luque, B. Shi and B. F. F. Sels, *Green Chem.*, 2023, **25**, 993–1003.
54 T. Pang, G. Wang, H. Sun, L. Wang, Q. Liu, W. Sui, A. M. Parvez and C. Si, *ACS Sustainable Chem. Eng.*, 2020, **8**, 9174–9183.
55 W. Zhao, L.-P. Xiao, G. Song, R.-C. Sun, L. He, S. Singh, B. A. Simmons and G. Cheng, *Green Chem.*, 2017, **19**, 3272–3281.
56 C. E. de Araujo Padilha, C. C. Nogueira, S. C. Bivar Matias, J. D. Barreto Costa Filho, D. F. de Santana Souza, J. A. de Oliveira and E. S. dos Santos, *Colloids Surf., A*, 2020, **603**, 125260.
57 M. H. Tran, D.-P. Phan and E. Y. Lee, *Green Chem.*, 2021, **23**, 4633–4646.
58 B. Wang, D. Sun, H.-M. Wang, T.-Q. Yuan and R.-C. Sun, *ACS Sustainable Chem. Eng.*, 2019, **7**, 2658–2666.
59 P. Figueiredo, K. Lintinen, J. T. Hirvonen, M. A. Kostiainen and H. A. Santos, *Prog. Mater. Sci.*, 2018, **93**, 233–269.
60 R. Lou, R. Ma, K.-t. Lin, A. Ahamed and X. Zhang, *ACS Sustainable Chem. Eng.*, 2019, **7**, 10248–10256.
61 N. F. Gajardo-Parra, V. P. Cotroneo-Figueroa, P. Aravena, V. Vesovic and R. I. Canales, *J. Chem. Eng. Data*, 2020, **65**, 5581–5592.
62 H. Zeng, B. Liu, J. Li, M. Li, M. Peng, C. Qin, C. Liang, C. Huang, X. Li and S. Yao, *Bioresour. Technol.*, 2022, **351**, 126951.
63 L. Liu, B. J. Liu, X. Y. Li, Z. L. Wang, L. L. Mu, C. R. Qin, C. Liang, C. X. Huang and S. Q. Yao, *Ind. Crops Prod.*, 2023, **200**, 116811.
64 J.-Q. Wu, J.-L. Wen, T.-Q. Yuan and R.-G. Sun, *J. Agric. Food Chem.*, 2015, **63**, 1763–1772.
65 X. Meng, C. Crestini, H. Ben, N. Hao, Y. Pu, A. J. Ragauskas and D. S. Argyropoulos, *Nat. Protoc.*, 2019, **14**, 2627–2647.
66 Z. Yan, G. Liao, X. Zou, M. Zhao, T. Wu, Y. Chen and G. Fang, *J. Agric. Food Chem.*, 2020, **68**, 8341–8349.
67 Y.-H. Xu, M.-F. Li and F. Peng, *Chem. Eng. J.*, 2023, **473**, 145233.